THE PENNSYLVANIA STATE UNIVERSITY
SCHREYER HONORS COLLEGE

DEPARTMENT OF MECHANICAL ENGINEERING

Overall Film Cooling Effectiveness on a Turbine Vane in Transonic Conditions

ISABELLA GAYOSO
SPRING 2023

A thesis
submitted in partial fulfillment
of the requirements
for baccalaureate degrees
in Mechanical Engineering and Aerospace Engineering
with honors in Mechanical Engineering

Reviewed and approved* by the following:

Stephen Lynch
Associate Professor of Mechanical Engineering
Thesis Supervisor

Margaret Byron
Assistant Professor of Mechanical Engineering
Honors Adviser

* Electronic approvals are on file.

ABSTRACT

In this experiment, measurements of the overall cooling effectiveness for a film cooled turbine vane airfoil in a high-speed cascade were obtained using infrared thermography. The vane used was the NASA C3X with impingement holes (showerhead cooling) and convective cooling holes on both the suction and pressure side. This work was done in the Mechanical Engineering Department's Experimental and Computational Convection Lab and used the high-speed cascade capability of the lab. The rationale for conducting this work was to obtain experimental data on film cooling effectiveness in a turbine vane in engine-like conditions at transonic speeds. Previous work has been done at subsonic speeds, but few pieces of literature examine this parameter at transonic speeds. The data can then be used to validate or compare to CFD models and to better understand what happens to the vane temperature distribution during engine operation. This understanding could inform the design of film cooling holes to reduce thermal strain "hot spots" which lead to failure of the vane. The results showed that trends for values of overall film effectiveness were as expected in this experiment, such as increases in blowing ratio correlating to increases in overall film effectiveness. However, the blowing ratios used in this study were not as high as values studied previously, indicating a need for more data on overall film effectiveness at transonic speeds.

TABLE OF CONTENTS

NOMENCLATURE iii

LIST OF FIGURES iv

LIST OF TABLES v

ACKNOWLEDGEMENTS vi

Chapter 1: Introduction 1

Chapter 2: Literature Review 6

Chapter 3: Experimental Methods and Procedures 11

Design Overview 13
Data Collection and Processing 22

Chapter 4: Results and Discussion 28

Chapter 5: Conclusions 37

BIBLIOGRAPHY 38

ACADEMIC VITA 41

NOMENCLATURE

Bi = Biot Number

c = vane chord

d = film cooling hole diameter

DR = Density ratio

h = Heat transfer coefficient

H = spanwise height of vane

I = Momentum flux ratio

M = Blowing ratio

p = film cooling hole pitch

q''_f = heat flux

r = radius of curvature

s = streamwise direction

T = Temperature

U = Velocity

VR = Velocity ratio

z = spanwise direction

Greek Symbols:

ϕ = Overall film effectiveness

η = Adiabatic film effectiveness

ρ = density

χ = Internal coolant warming factor

Subscripts:

c = coolant flow properties

f = with film cooling

i = internal state

∞ = mainstream conditions

0 = without film cooling

w = wall conditions

LIST OF FIGURES

Figure 1. Overall Facility Layout....11

Figure 2. Exploded View of Test Section....12

Figure 3. Test Section with Blade Assembly and Instrumentation....12

Figure 4. Exploded View of Test Assembly....13

Figure 5. CAD Model of Linear Cascade....14

Figure 6. Labeled Cross Section of Vane....15

Figure 7. Coordinate System and Film Cooling Holes Locations....16

Figure 8. Vane Geometry, Proportional Holes....18

Figure 9. Vane Geometry, Larger Holes....19

Figure 10. Additively Manufactured Test Vane....22

Figure 11. Airfoil Pressure Loading....23

Figure 12. T_∞ and $T_{c,i}$ vs Time (sec) for PS at Low M....25

Figure 13. Spatial Calibration of IR image....26

Figure 14. Raw IR Images of Vane Suction Side....28

Figure 15. Vane SS Surface Temperature at High, Med, and Low M....29

Figure 16. Vane SS Overall Film Effectiveness at High, Med, and Low M....30

Figure 17. Raw IR Images of Vane Pressure Side....31

Figure 18. Vane PS Surface Temperature at High, Med, and Low M....31

Figure 19. Vane PS Overall Film Effectiveness at High, Med, and Low M....33

Figure 20. $\boldsymbol{\phi}$ vs (s/s_{max}) for all Measured Blowing Ratios....34

Figure 21. $\boldsymbol{\phi}$ vs (s/d) for all Measured Blowing Ratios....35

Figure 22. $\boldsymbol{\phi}$ vs (s/d) from the Results of Nathan, et al. [3]....36

LIST OF TABLES

Table 1. Showerhead Film Cooling Hole Geometry Used in Nathan et al., 2013 [3] 16

Table 2. Positions of Showerhead Film Cooling Holes – Proportionally Scaled Geometry....17

Table 3. Positions of Larger Film Cooling Holes in Final Geometry.....19

Table 4. Position of Convective Film Cooling Holes 20

Table 5. Design vs Actual Hole Diameters.....21

Table 6. Test Matrix for SS with Projected Blowing Ratios.....24

Table 7. Test Matrix for PS with Projected Blowing Ratios.....24

Table 8. Corresponding M* for I* from values used in Nathan, et al. [3].....35

ACKNOWLEDGEMENTS

First and foremost, I would like to express my sincerest gratitude to Dr. Stephen Lynch for his guidance throughout the process. Thank you for welcoming me into the lab and patiently teaching me new technical skills throughout the semesters. I really enjoyed learning about the topics studied and find it one of the most important experiences of my undergraduate education. I also want to extend that gratitude to Andrew Fox, who was instrumental in helping me with the experimental process and answering my many questions, and all the graduate students in the Experimental and Computational Convection Laboratory (ExCCL) for everything they have taught me. I also want to thank my honors advisor, Dr. Margaret Byron, for her support and advice throughout the process. Lastly, a huge thank you to my friends and family for their continuous support throughout my undergraduate education.

Chapter 1: Introduction

The rationale for conducting this work is to obtain experimental data on overall film cooling effectiveness in a turbine vane in engine-like conditions. This can then be used to validate or compare to CFD models. It can also be used to better understand what happens in a vane in an engine during operation. This understanding could be used to improve the design of film cooling holes to reduce hot spots that could lead to failure of the vane.

In modern gas turbines/jet engines, operating temperatures often exceed critical material temperatures of turbine blades and vanes. As a result, the hardware needs to be cooled to prevent structural failure. Current cooling methods are a combination of internal cooling and external cooling on the surface of the blade, called film cooling. Internal cooling consists of internal channels of colder air being flowed through the vane or blade. Film cooling is achieved by blowing out colder air through holes on the vane in the direction of flow. This creates a layer of colder temperature air on the surface of the blade, which as a result reduces the overall blade surface temperature and internal temperature.

Film cooling performance is often measured by Adiabatic Film Effectiveness and Overall Film Cooling Effectiveness. Adiabatic film effectiveness is a nondimensional representation of the adiabatic wall temperature, which can be thought of as the average gas temperature above the airfoil surface with the introduction of a cooling film so that it is somewhere between the hot gas temperature and the cooling temperature as the coolant jet mixes with the gas downstream of injection. It is typically normalized in a form like [Equation 1]. In situations of attached film cooling, the adiabatic film temperature is the most appropriate reference temperature when

calculating the heat transfer through a turbine blade wall but is difficult to measure in practice since it requires an adiabatic (non-conducting) surface. Some low thermal conductivity materials can approximate adiabatic conditions (such as foam) but any real surface has non-zero thermal conductivity, making this a difficult parameter to measure.

$$\eta = \frac{T_\infty - T_{aw}}{T_\infty - T_{c,exit}} \qquad [Equation\ 1]$$

In contrast, overall film cooling effectiveness indicates how effectively the surface is cooled relative to the mainstream flow temperature by directly measuring external wall temperature, T_w. [Equation 2]. In this case, convection occurring in internal channels inside the model, conduction of heat through the metallic wall, and convection occurring on the outer surface, all play a role in determining the outer wall temperature. This parameter can be more closely related to the actual temperature of a turbine blade in operation if the appropriate non-dimensional parameters are matched between the lab scale and engine scale.

$$\phi = \frac{T_\infty - T_w}{T_\infty - T_{c,i}} \qquad [Equation\ 2]$$

To estimate heat transfer to the vane surface, the heat transfer coefficient with film cooling, h_f, must be found using [Equation 3], which is the equation for heat flux. The heat transfer coefficient is often expressed in ratio to the heat transfer coefficient without film cooling, h_0. The heat transfer coefficient augmentation factor is written as h_f/h_0. Generally, this ratio is around 1.1 to 1.4 depending on the type of hole and distance from injection.

$$q_f^{"} = h_f(T_{aw} - T_w) \qquad [Equation\ 3]$$

To match engine-like conditions, previous literature utilizes the Biot Number (Bi). The Biot Number is a function of h_f, thermal conductivity, k, and the thickness of the vane, t. This approach achieves representative conditions by scaling thermal conduction through the vane

body to match the condition experienced in an engine. As a result, the normalized surface temperature, ϕ, would be the same as on an actual vane, allowing for direct measurement of the temperature distribution on an airfoil. The measurement can be used to understand the thermal stresses and "hot spots" on a vane. [Equation 4] represents a 1D heat transfer analysis of a film cooled wall with an internal wall heat transfer coefficient of h_i and an external wall coefficient of h_f.

$$\phi = \frac{1 - \chi\eta}{1 + Bi + \frac{h_f}{h_i}} + \chi\eta \qquad [Equation\ 4]$$

The internal coolant warming factor, χ, adjusts for the difference in coolant temperatures between the entrance and exit of the film cooling passages, as shown in [Equation 5]. If the Reynolds number and internal passage geometry of a laboratory experiment are matched to representative conditions, the internal coolant warming factor should be similar as well. The heat transfer coefficient augmentation factor h_f/h_i should also match engine-like conditions and can be achieved through proper internal cooling design.

$$\chi = \frac{T_\infty - T_{c,f}}{T_\infty - T_{c,i}} \qquad [Equation\ 5]$$

The advantage of measuring overall film cooling effectiveness and matching engine parameters is that ϕ accounts for adiabatic film cooling effectiveness, conjugate heat transfer effects from internal and external cooling, and altered heat transfer coefficients. This eliminates the problem of trying to directly measure film cooling effectiveness in a dense region of cooling, like in a showerhead cooling configuration [10].

Blowing ratio (M) is most used in literature as it measures flow rate and heat capacity of the flow, shown in Equation 6. Blowing ratio is correlated with jet attachment from film cooling holes, with lower values having more attached flows.

$$M = \frac{(pU)_{coolant}}{(pU)_{\infty}} \qquad [Equation\ 6]$$

Momentum flux ratio (I) is an alternative measurement to blowing ratio and measures the ability to turn coolant jets toward the wall using the mainstream flow.

$$I = \frac{(pU^2)_{coolant}}{(pU^2)_{\infty}} \qquad [Equation\ 7]$$

Another important set of parameters are the velocity ratio (VR) and density ratio (DR). Velocity ratio matches velocity gradients without considering the effects of density (Equation 8). Density ratio does the opposite, matching the density ratio of the coolant and mainstream flows as shown in Equation 9 [10].

$$VR = \frac{U_{coolant}}{U_{\infty}} \qquad [Equation\ 8]$$

$$DR = \frac{\rho_{coolant}}{\rho_{\infty}} \qquad [Equation\ 9]$$

Film cooling performance is often tied to the size, shape, spacing, and orientation of the holes. For the first few decades of film cooling technology, circular holes were used since they are simple to manufacture (requires a single drilling process in the turbine blade). Many studies could be conducted at matched nondimensional parameters and be relevant to the engine condition. However, circular holes suffer from film detachment at high cooling flowrates, which degrades their performance significantly. A more recent development was the use of an expanded outlet to the hole, much like a diffuser, to slow down the film and keep it attached to the surface. These are known as shaped film cooling holes and have also received a lot of

attention. Most recently with the introduction of CFD and computational optimization solvers, the most efficient hole design may no longer be cylindrical, but instead have shaped or non-circular geometries. At transonic speeds, which more closely resembles engine-like conditions, this creates a shock and other turbulent flow in the film cooling holes that needs to be characterized experimentally, which is a large part of the exigence for this study.

Chapter 2: Literature Review

Previous work done on film cooling effectiveness of cylindrical film cooling holes in the showerhead region has shown a large reduction in surface temperatures when film cooling was used. Mick and Mayle [6] showed that heat transfer coefficients near the surface were reduced as much as three times while downstream the reduction decreased to a 10% reduction. Using blowing ratios ranging from M = 0.4 to M = 1.2, they also found adiabatic film effectiveness decreased near the leading edge due to film blowoff but increased downstream as blowing ratio increased.

Another study conducted by Cutbirth and Bogard [7] also concluded that adiabatic film effectiveness increased with blowing ratio and tested ratios from M_{sh} = 0.8 to M_{sh} = 1.5. This study utilized an infrared camera instead of thermocouple arrays like Mick and Mayle [6] and captured the separation of coolant jets from the surface in the showerhead region. Despite this separation, it was noted that between blowing ratios M_{sh} = 1.0 and M_{sh} = 1.5 there is a sudden increase in η due to the coolant jet interaction with laterally adjacent holes which prevented mainstream flow from reaching the surface.

The parameter matching technique mention in the introduction of this paper is utilized in Albert, et al. [8] to directly measure overall film cooling effectiveness and study the conjugate heat transfer of internal convection and external conduction on the blade surface. In addition, the experiment also measured η and compared ϕ over a blowing ratio range from M = 1.0 to 4.0. While η decreased dramatically between coolant holes near the stagnation line, ϕ remained relatively constant, which was a notable difference and represented conjugate heat transfer in

engine-like conditions. After M = 2.6, increases in blowing ratio did not have a significant effect on overall cooling effectiveness.

Recent work in overall effectiveness in the showerhead region of a turbine vane has mostly been conducted in subsonic conditions. Nathan, et al. [3] utilized a NASA C3X vane model from Hylton. et al. [2] with five rows of impingement holes (showerhead cooling) and one row of film cooling on each the pressure side and suction side. By measuring overall film cooling effectiveness with Biot number matching at subsonic conditions, the study was able to identify "hot spots" in a vane with showerhead cooling. This is significant because due to parameter matching, the results are representative of "hot spots" that would lead to failure in real engine conditions. Another important conclusion drawn from this study is that staggering showerhead holes could lead to gaps in adiabatic film effectiveness. Therefore, positioning holes to prevent gaps in the adiabatic film cooling effectiveness is important to prevent "hot spots".

However, as previously mentioned, measuring adiabatic film effectiveness directly is more challenging than measuring overall film cooling effectiveness. As a result, experiments have been conducted to evaluate the cooling effects of internal cooling alone, and then the combined effects of film cooling and internal cooling for a range of coolant flow rates. In Williams, et al. overall cooling effectiveness and adiabatic film effectiveness were measured at subsonic speeds downstream of a single row of round holes positioned on the suction side of the vane (with two rows on the pressure side) [4]. Surface temperature showed higher variation at lower flow rates for local values of both η and ϕ.

Predictive modeling did not match the experimental results in Williams, et al., which is why this paper aims to provide further insight into the local surface values of ϕ, especially at transonic Mach numbers. It was shown the assumption of 1D heat transfer used to derive

[Equation 4] failed to provide a close estimate of ϕ for both detached and attached jets. This conclusion is also supported by Dyson, et al., where CFD over-predicted both η and ϕ for attached jets, and under-predicted both adiabatic and overall effectiveness for detached jets [1]. Adiabatic wall temperature, T_{aw}, was also determined to not be an appropriate driving temperature for heat transfer, especially in the case of a detached jet. CFD often does not properly predict real-life results, as demonstrated in Dyson, et al. [1] Therefore, experimentally obtained measurements are important for understanding real engine conditions and validating computation models.

Using computational modeling and optimization, shaped (rather than circular) film cooling holes that prevent coolant jet separation from the surface could be the optimal design to achieve the best film cooling performance. This topic was examined in Bacci, et al. Using fan shaped film cooling holes tested at a Mach number of 0.54, the study found nominal cylindrical hole correlations vastly overpredicted the adiabatic film cooling effectiveness on the pressure side across blowing ratios from M = 1.0 to 2.5 [9].. On the suction side, correlations of η in cylindrical hole geometries are similar except in the final row of holes located towards the aft end of the airfoil, in which η was also overpredicted, especially for blowing ratios above M = 1.5. Overall, this study demonstrated the differences in adiabatic film effectiveness of shaped holes compared to cylindrical holes. Several factors could be the cause for these differences, including the scaling parameters used. A study by Anderson, et al. examined various scaling parameters and found the velocity ratio, VR, is the best scaling parameter for both cylindrical and shaped holes as opposed to blowing ratio, M, which has most commonly been used in literature for parameter matching [10]. Additionally, it was noted this is due to large turbulence

generation dispersing coolant when the velocity gradient between the coolant jets and mainstream flow is significant.

Furthermore, Mach number of the flow near the hole exit greatly impacts film effectiveness. This topic was explored in Ligrani, et al. in cylindrical holes and determined to be due to shock formation at transonic Mach numbers [11]. The generation of oblique shock waves and deflection cause adiabatic film effectiveness to increase when shocks are present near the exit of the holes. As shown in Gritsch, et al., transonic flow near the film hole exits increased adiabatic film effectiveness for cylindrical and shaped holes when inlet flow Mach number was subsonic [12]. However, increasing coolant flow Mach number (up to 0.6) near the entrance of the film holes was shown to increase adiabatic film effectiveness in cylindrical holes. But on the other hand, the shaped holes saw a large reduction in η with inlet coolant Mach numbers increases due to disturbances in the flow which prevents lateral diffusion of coolant flow.

Although Mach number and velocity ratio have a significant impact on film cooling performance, few studies measure overall film effectiveness, ϕ, at transonic speeds representative of engine parameters. This study aims to provide an experimental dataset of overall film cooling effectiveness in turbine vanes at transonic speeds to better understand the performance and key differences of showerhead film cooling holes at these speeds. Additionally, overall film effectiveness measurements collected in this experiment are compared to the results of similar geometry tested at subsonic speeds.

Chapter 3: Experimental Methods and Procedures

This experiment was conducted using the steady, transonic linear cascade at the Penn State ExCCL Lab, which utilizes the high-flow compressor (1.1 MW) from the Penn State START Lab capable of supplying a mass flow rate of 5.4 kg/s (12 lbm/s) [5].

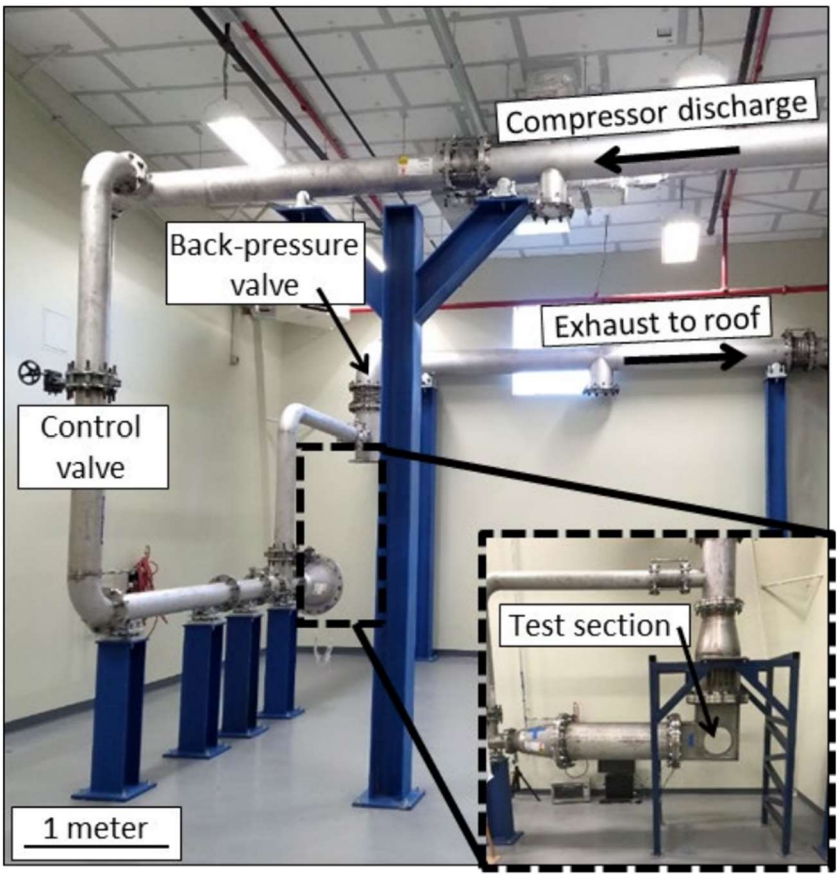

Figure 1. Overall Facility Layout

Source: Zuccarello, et al. [5]
Copyright 2020 by ASME and United Technologies Corporation. Reprinted with permission.

Coolant was supplied to vane cavities using the cascade loop (opened by the control valve shown in Figure 1), and all coolant was exhausted out the film cooling holes in each cavity.

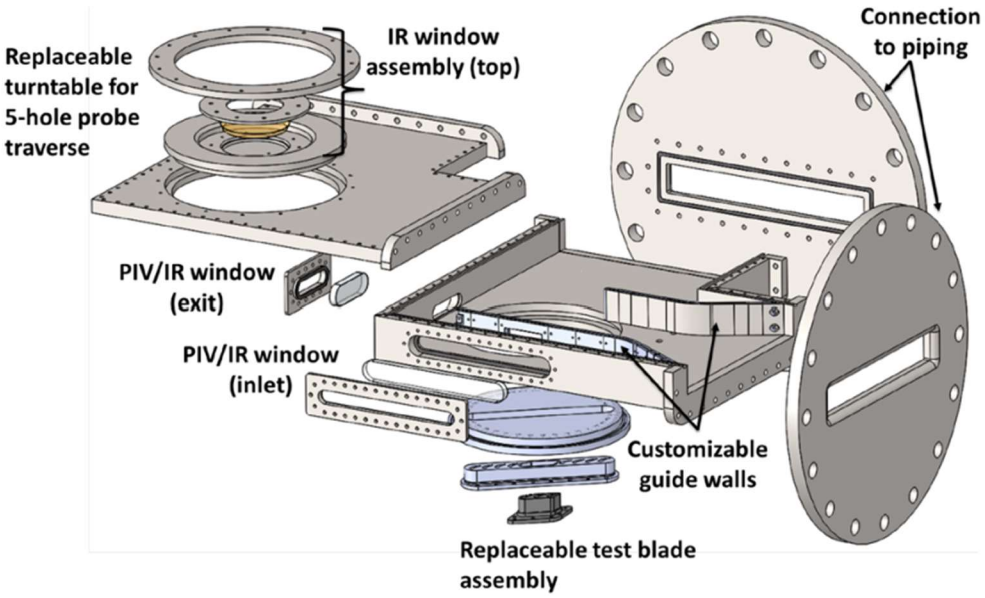

Figure 2. Exploded View of Test Section

Source: Zuccarello, et al. [5]
Copyright 2020 by ASME and United Technologies Corporation. Reprinted with permission.

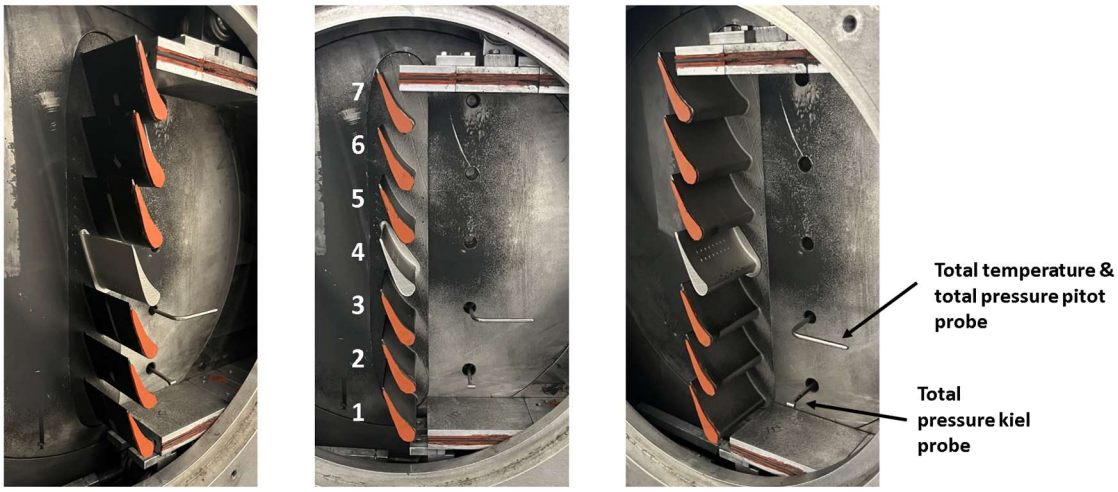

Figure 3. Test Section with Blade Assembly and Instrumentation

The test section consists of a test blade assembly with a replaceable center vane placed inside a metal box with viewing windows for the infrared (IR) camera, ports for instrumentation, and connections to piping. Using a FLIR A615 IR camera, measurements of the vane surface

temperature were obtained. Spatial calibration of the IR camera was performed so that temperature measurements can be extracted from the IR images in data processing. The value used for $T_{c,i}$ came from thermocouple measurements in the vane cavities. Pressure measurements were obtained using pressure taps placed in the vane cavities (Figure 6).

Figure 4. Exploded View of Test Assembly

Design Overview

This study used the NASA C3X vane from Hylton, et al. [2]. To fit existing lab hardware and manufacturing constraints, the vane was scaled to 0.0965 times the original size and placed in the cascade, pictured in Figures 4 and 5.

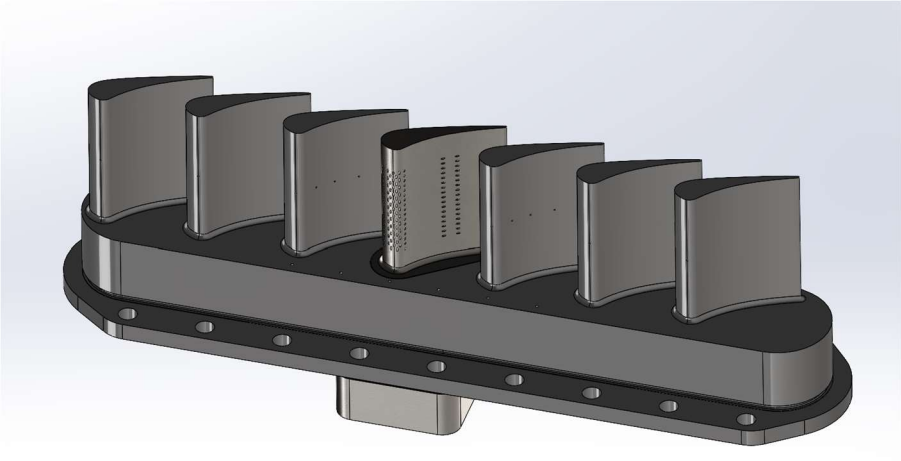

Figure 5. CAD Model of Linear Cascade

To supply coolant flow, two cavities were modeled in the vane. The first cavity supplies coolant to the showerhead film cooling holes, and the second cavity supplies coolant to the convective cooling holes. Both cavities have a pressure tap hole and thermocouple hole, labeled in Figure 6.

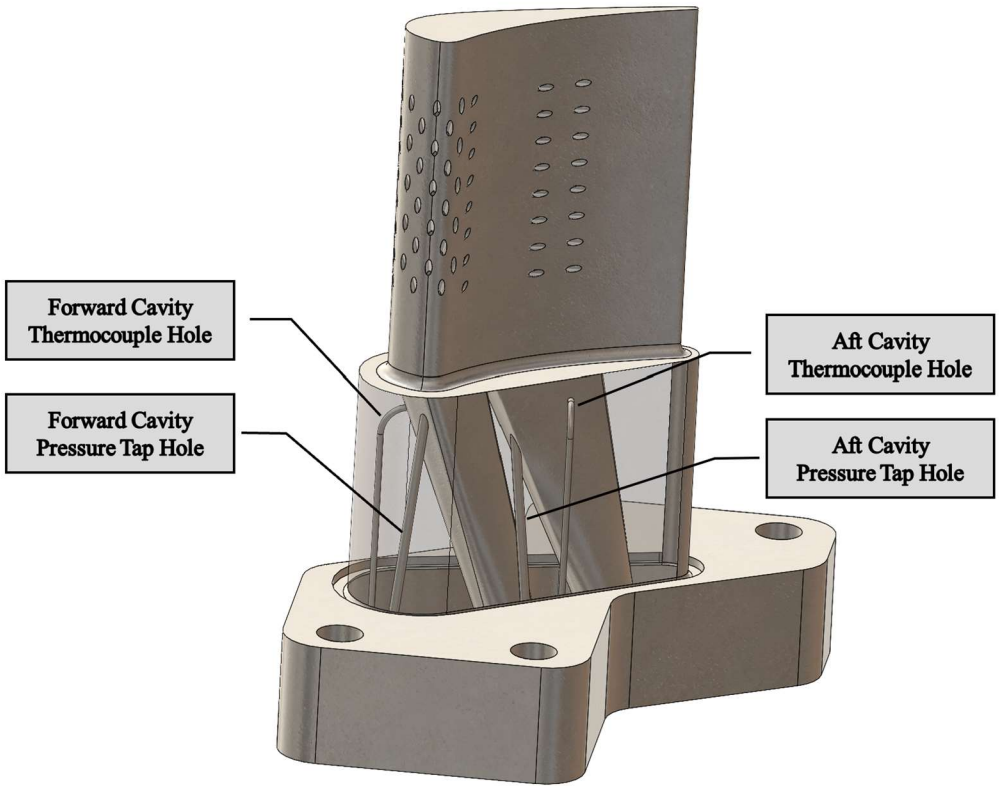

Figure 6. Labeled Cross Section of Vane

In this study, a cooling geometry similar to the geometry from Nathan, et al. was used [3]. This configuration consisted of seven rows of cooling holes (showerhead cooling), as described in detail in Table 1. The showerhead rows each had five circular holes. The PS1 and SS1 rows had eight holes [3]. An overview of the film cooling hole locations is provided in Figure 7.

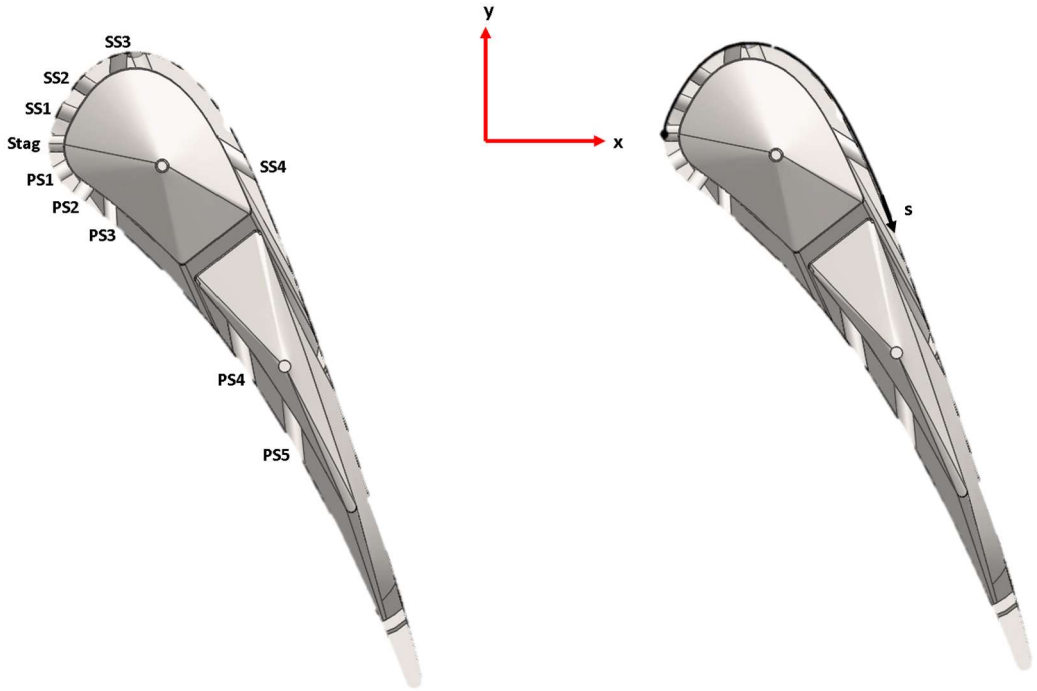

Figure 7. Coordinate System and Film Cooling Holes Locations

Table 1. Showerhead Film Cooling Hole Geometry Used in Nathan et al., 2013 [3]

Row Name	Position (s/d)	Surface angle (deg)	Compound angle (deg)	d (mm)	Pitch (p/d)
PS1	-8.0	30	60	4.76	5.33
SH-PS2	-4.0	25	90	6.35	6
SH-PS1	-2.0	25	90	6.35	6
SH-Stag	0.0	25	90	6.35	6
SH-SS1	2.0	25	90	6.35	6
SH-SS2	4.0	25	90	6.35	6
SS1	7.0	35	68	6.35	4

The NASA C3X vane was originally scaled down from a height of 547 mm as used in Nathan, et al. to a height of 52.83 mm (2.08 in) to fit existing facility capabilities [3]. The

geometry in this study was scaled proportionally and is described in Table 2. Position and pitch are a function of film hole diameter, which was scaled proportionally to the height. The suction side and showerhead row hole diameters were scaled from 6.35 mm to 0.613 mm (0.0241 inches). The pressure side row holes were scaled from 4.76 mm to 0.460 mm (0.0181 inches), as shown in Figure 8.

$$Ratio = \frac{52.83}{547} = 0.0965 \qquad [Equation\ 6]$$

$$Ratio = \frac{0.613}{6.35} = 0.0965 \qquad [Equation\ 7]$$

$$Ratio = \frac{0.460}{4.76} = 0.0967 \qquad [Equation\ 8]$$

Table 2. Positions of Showerhead Film Cooling Holes – Proportionally Scaled Geometry

Row Name	Position (s/d)	Surface angle (deg)	Compound angle (deg)	d (in)	Pitch (p/d)
PS3	-8.0	30	60	0.0181	5.33
PS2	-4.0	25	90	0.0241	6
PS1	-2.0	25	90	0.0241	6
Stag	0.0	25	90	0.0241	6
SS1	2.0	25	90	0.0241	6
SS2	4.0	25	90	0.0241	6
SS3	7.0	5	68	0.0241	4

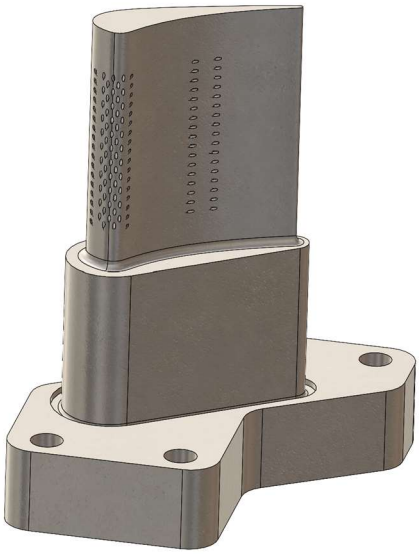

Figure 8. Vane Geometry, Proportional Holes

However, due to limitations of the additive manufacturing process, the smallest hole diameter was assumed to be limited to at least a minimum of 0.030 inches. Therefore, the hole diameters were adjusted to be larger, as shown in Figure 9. The pressure side row hole diameter was scaled to 0.030 inches. To keep the same proportion between the hole sizes, the suction side and showerhead row holes were scaled to 0.040 inches, as outlined in Table 3. All other values (position, surface angle, compound angle, and pitch) remain consistent with Nathan, et al. [3]. Equation 9 shows the hole diameter ratios from Nathan, et al. [3]. Equation 10 shows the hole diameter ratios of the proportionally scaled geometry. Equation 11 shows the hole diameter ratios of the final geometry with hole sizes adjusted for the additive manufacturing process.

$$Ratio = \frac{4.76}{6.35} = 0.750 \qquad [Equation\ 9]$$

$$Ratio = \frac{0.0181}{0.0241} = 0.751 \qquad [Equation\ 10]$$

$$Ratio = \frac{0.0300}{0.0400} = 0.750 \qquad [Equation\ 11]$$

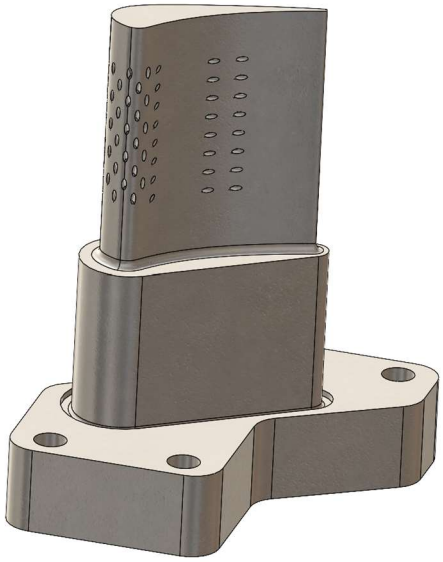

Figure 9. Vane Geometry, Larger Holes

Table 3. Positions of Larger Film Cooling Holes in Final Geometry

Row Name	Position (s/d)	Surface angle (deg)	Compound angle (deg)	d (in)	Pitch (p/d)
PS3	-8.0	30	60	0.030	5.33
PS2	-4.0	25	90	0.040	6
PS1	-2.0	25	90	0.040	6
Stag	0.0	25	90	0.040	6
SS1	2.0	25	90	0.040	6
SS2	4.0	25	90	0.040	6
SS3	7.0	5	68	0.040	4

The precise placement of pressure side convective cooling holes is not stated in Nathan, et al. [3], however it is mentioned “the design of the aft passage holes is unimportant to the current study”. In this geometry configuration, the pressure side holes were placed in the center of the aft cavity, allowing for distance from the cavity wall on either end. The nondimensional positions are called out in Table 3.

The suction side convective cooling holes are mentioned to be at a stagnation line of *s/c* = 0.512 in another paper by Williams et al. [4]. Using an original true chord of 531 mm and scaling proportionally to this geometry configuration gives a chord of 51.24 mm (2.017 in). Solving for *s*, the position along the vane, the result is 26.24 mm (1.033 in). The nondimensional position (*s/d*) is then found to be 25.83. However, due to cavity wall constraints, the SS2 convective cooling holes were placed further forward at a position of s/d=19.25, as shown in Table 3.

Table 4. Position of Convective Film Cooling Holes

Row Name	Position (s/d)	Surface angle (deg)	Compound angle (deg)	d (in)	Pitch (p/d)
PS4	-17.5	25	0	0.040	4
PS5	-24.5	25	0	0.040	4
SS4	19.25	25	0	0.040	4

Matching the hole geometry in Nathan, et al., the convective cooling holes have a compound angle of 0 degrees, pitch (p/d) of 4, and a surface angle of 25 degrees [3]. The diameter was chosen to be 0.040 inches to match the showerhead hole diameter sizes. The pressure side has two rows, and the suction side has one row. Each row (PS2, PS3, and SS2) has eight holes.

The vane was additively manufactured using Direct Metal Laser Sintering (DMLS) from Xometry and is made of Stainless Steel 316L. As a result, the actual hole diameters were slightly smaller than the design diameters, as shown in Table 5. Hole sizes were determined using pin gauges placed in the part at each hole's respective angle to ensure that the pin gauges measured

hole size despite the surface angle. The holes were relatively clear and unobstructed, as was determined by usage of the pin gauges (shown in Figure 10).

Table 5. Design vs Actual Hole Diameters

Row Name	Design d (in)	Actual d (in)
PS5	0.040	0.024
PS4	0.040	0.024
PS3	0.030	0.018
PS2	0.040	0.030
PS1	0.040	0.030
Stag	0.040	0.030
SS1	0.040	0.030
SS2	0.040	0.030
SS3	0.040	0.030
SS4	0.040	0.023

(a)  (b) 

(c)  (d) 

Figure 10. Additively Manufactured Test Vane

Data Collection and Processing

The flow field was verified prior to data collection and is shown in Figure 11. In the figure, the dots are experimentally measured surface pressures, and the line is a computational fluid dynamics (CFD) prediction for the airfoil at the desired exit Mach number of 0.9. The airfoil pressure loading distribution on the suction and pressure surfaces of the vane matches the expected behavior for the test conditions (Ma = 0.9).

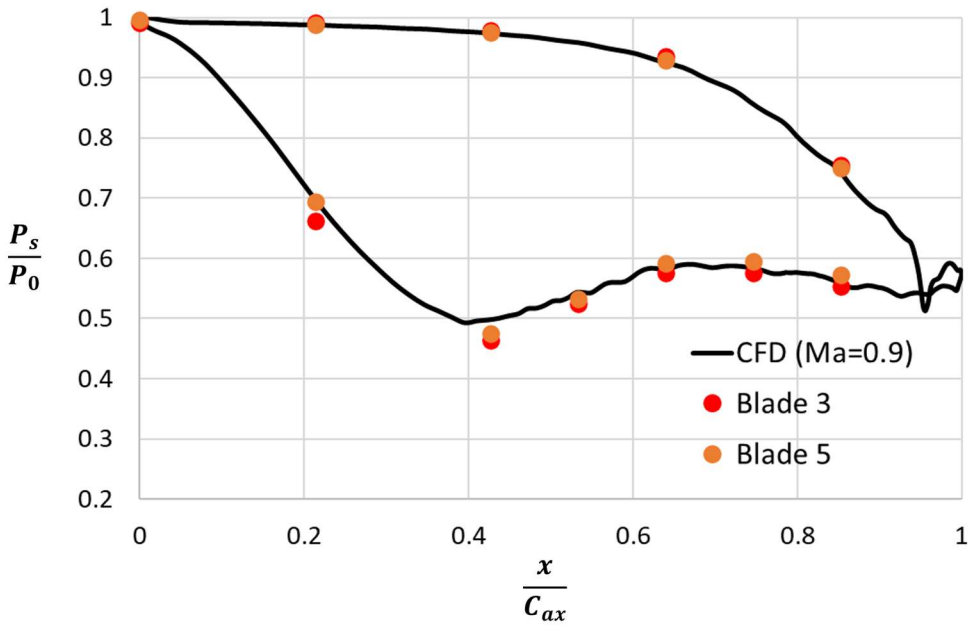

Figure 11. Airfoil Pressure Loading

The test matrix shown in Table 6 and Table 7 shows the projected blowing ratios (for the designed hole diameters) achieved by adjusting the mass flow rate of the coolant supply. Target blowing ratios were restricted by the mass flow rate supply capability of the facilities and the vane geometry, which supplied coolant to several holes from the leading edge (LE) cavity, restricting the blowing ratio. Separate tests were conducted on the suction side and pressure side due to the positioning of the IR camera only allowing one side to be imaged at a time. Different mass flow rates were selected to allow for a range in the M achieved through each hole row. The mass flow rates tested on the SS were $\dot{m} = 1.2$, $\dot{m} = 1.8$, and $\dot{m} = 2.4$, all in g/s. The mass flow rates tested on the PS were $\dot{m} = 0.8$, $\dot{m} = 1.6$, and $\dot{m} = 2.4$, all in g/s.

Table 6. Test Matrix for SS with Projected Blowing Ratios

Channel	Hole row	Low M			Medium M			High M		
		Test No.	ṁ (g/s)	M	Test No.	ṁ (g/s)	M	Test No.	ṁ (g/s)	M
LE	SS4	Test #1	1.2	0.10	Test #2	1.8	0.15	Test #3	2.4	0.20
	SS3			0.10			0.15			0.21
	SS2			0.18			0.27			0.36
	SS1			0.29			0.43			0.57
	Stag	Test #1	1.2	0.00	Test #2	1.8	0.00	Test #3	2.4	0.00
	PS1			0.63			1.26			1.90
	PS2			0.34			0.69			1.03
	PS3			0.31			0.61			0.92
TE	PS4	Test #1	0.8	0.47	Test #2	1.6	0.94	Test #3	2.4	1.41
	PS5			0.34			0.67			1.01

Table 7. Test Matrix for PS with Projected Blowing Ratios

Channel	Hole row	Low M			Medium M			High M		
		Test No.	ṁ (g/s)	M	Test No.	ṁ (g/s)	M	Test No.	ṁ (g/s)	M
LE	SS4	Test #4	0.8	0.10	Test #5	1.6	0.15	Test #6	2.4	0.20
	SS3			0.10			0.15			0.21
	SS2			0.18			0.27			0.36
	SS1			0.29			0.43			0.57
	Stag	Test #4	0.8	0.00	Test #5	1.6	0.00	Test #6	2.4	0.00
	PS1			0.63			1.26			1.90
	PS2			0.34			0.69			1.03
	PS3			0.31			0.61			0.92
TE	PS4	Test #4	0.8	0.47	Test #5	1.6	0.94	Test #6	2.4	1.41
	PS5			0.34			0.67			1.01

Monitoring of target test conditions and data collection was done using LabVIEW, which allowed for organized data processing. Recordings of the vane surface temperature at different test conditions were obtained using the IR camera. Five stills were taken from each video. Figure 12 shows an example of the inlet coolant and mainstream (cascade inlet) temperature at the time each IR camera image was taken for the PS side at low M.

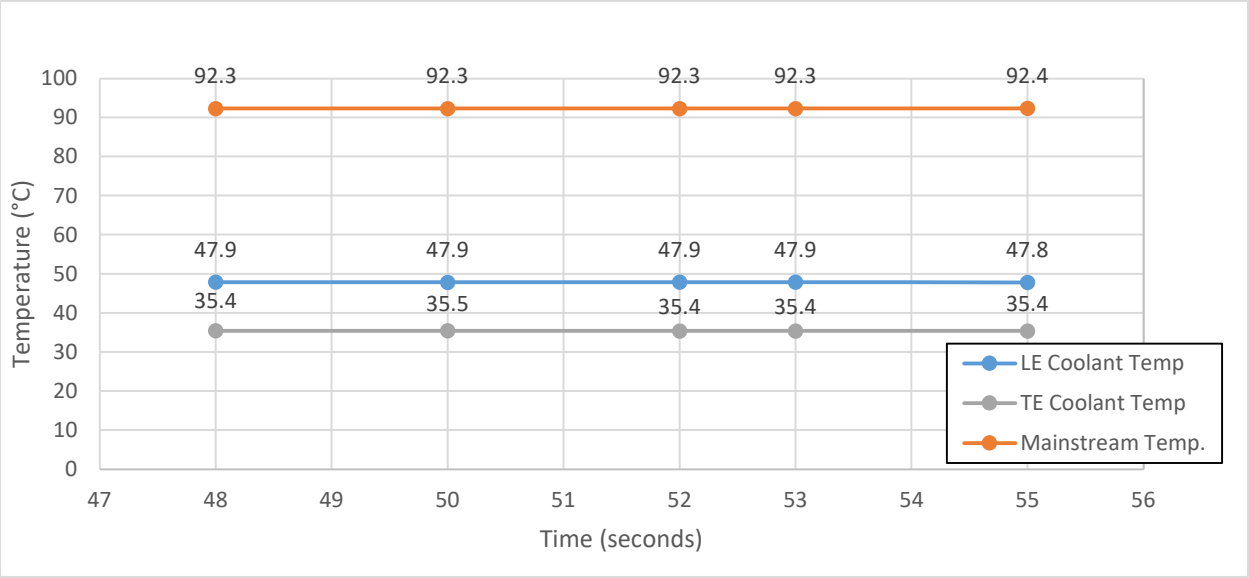

Figure 12. T_∞ and $T_{c,i}$ vs Time (sec) for PS at Low M

Using a specific software for the IR camera known as ThermaCam, the temperature measurements captured from each image were averaged into a single image that was converted to a MATLAB format. The coolant and mainstream temperature values from each IR image were also averaged. The x and y coordinates of each hole had to be correlated with the image pixel coordinates for spatial interpretation of temperature measurements. This process is illustrated in Figure 13.

Marker Labels	Xpos (in)	Ypos (in)	Xpos (m)	Ypos (m)	Xmark	Ymark
1,1	0	0	0	0	348	266
2,1	0.25	0	0.00635	0	315	259
3,1	0.5	0	0.0127	0	280	249
4,1	0.75	0	0.01905	0	247	241
5,1	1	0	0.0254	0	216	231
6,1	1.25	0	0.03175	0	185	219
1,2	0	0.25	0	0.00635	348	293
2,2	0.25	0.25	0.00635	0.00635	315	283
3,2	0.5	0.25	0.0127	0.00635	282	274

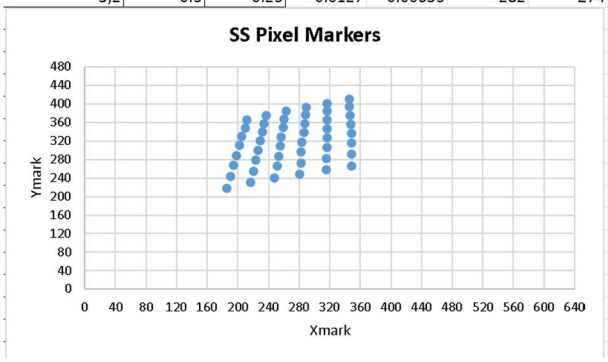

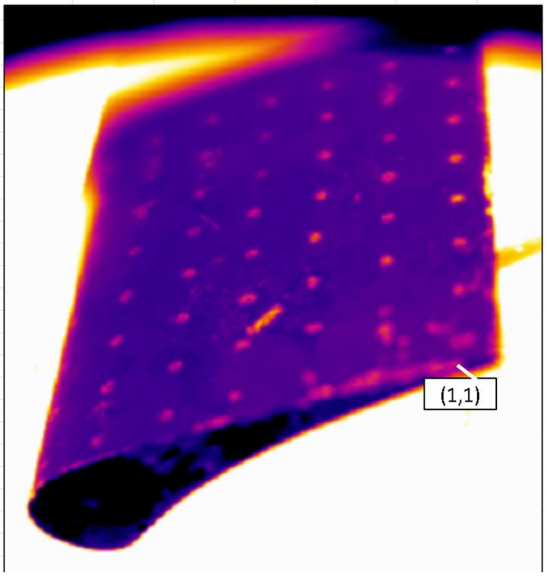

Figure 13. Spatial Calibration of IR image

In MATLAB, the vane surface coordinates at the known calibration point locations were correlated with the IR camera pixel coordinates to convert the IR temperature measurements at each location to a vane coordinate system, using a custom MATLAB code. The code also clips out data that is not part of the original image, organizes the remaining data for graphical interpretation, and applies the IR temperature calibration curve, shown in Equation 12 for the pressure side and Equation 13 for the suction side. Both IR_{actual} and IR_{camera} are in °C.

$$IR_{actual} = 0.9822.* (IR_{camera} - 273.15) + 0.4473 \qquad [Equation\ 12]$$

$$IR_{actual} = 0.9896.* (IR_{camera} - 273.15) + 0.0825 \qquad [Equation\ 13]$$

Overall film effectiveness (shown in Equation 2, Equation 4, and Equation 5) was found using the calibrated temperature values (IR_{actual}) measured by the IR camera and test conditions recorded during testing (T_∞ and $T_{c,i}$).

$$T_{\infty} = \ From\ averaged\ mainstream\ cascade\ temperature, \text{°C}$$

$$T_{c,i} = \ From\ averaged\ inlet\ coolant\ temperature, \text{°C}$$

$$T_{c,f} = \ From\ calibrated\ temperature\ values\ (IR_{actual}), \text{°C}$$

For the SS images (Tests #1-3), the average LE inlet coolant temperature was used for $T_{c,i}$. For the PS images (Tests #4-6), the average LE inlet coolant temperatures and the average TE inlet coolant temperatures were averaged and used for $T_{c,i}$. This is due to the pressure side holes utilizing coolant from both cavities, with PS1, PS2, and PS3 using coolant from the LE cavity and PS4 and PS5 using coolant from the TE cavity. For example, using the values from Figure 12 for the pressure side at low M, the values of $T_{c,i} = 41.653\ \text{°C}$ and $T_{\infty} = 92.343\ \text{°C}$ were used.

Chapter 4: Results and Discussion

Overall film cooling effectiveness results are presented for each the suction side and pressure side at low, medium, and high blowing ratios (as defined in the test matrix in Table 6 and Table 7). Raw IR images of the vane suction side indicate increased cooling on the surface at the highest value of M, which is consistent with findings of Nathan, et al. [3] in which overall cooling effectiveness increased with an increase in M.

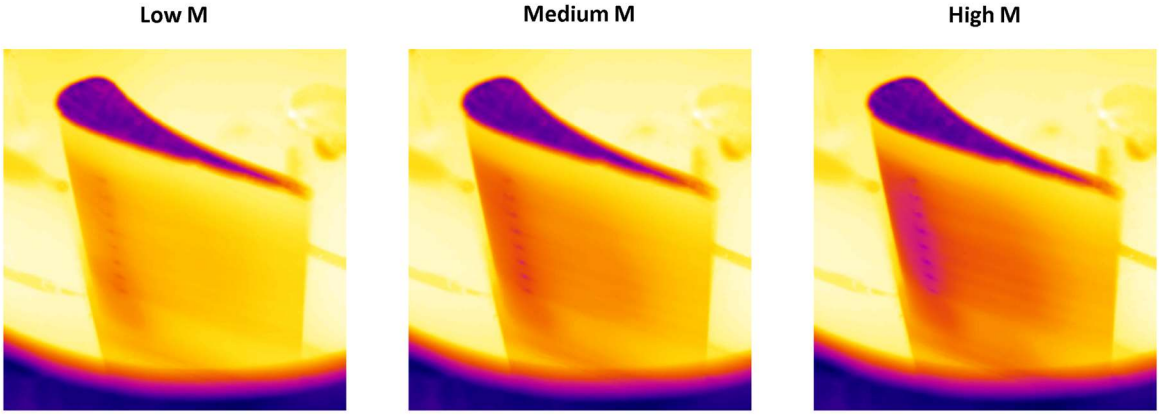

Figure 14. Raw IR Images of Vane Suction Side

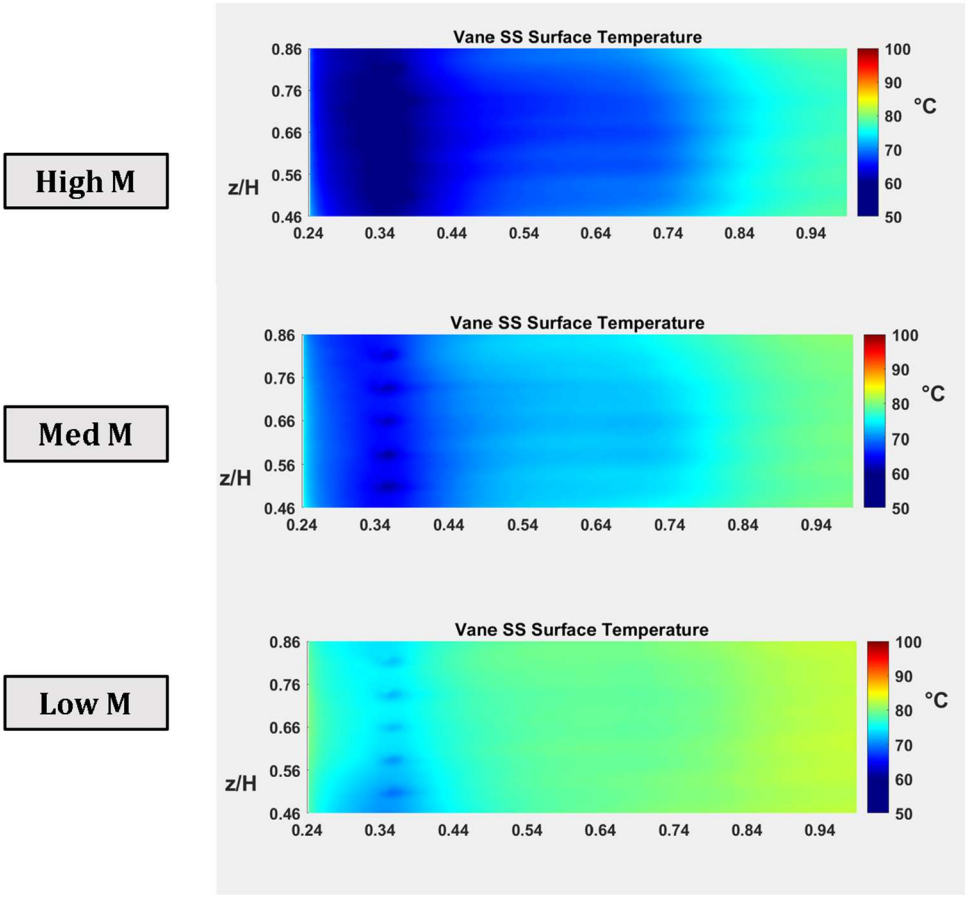

Figure 15. Vane SS Surface Temperature at High, Med, and Low M

From the suction side images, only one convective cooling hole is captured (SS4). Comparing the temperature contour plots (Figure 15), it is shown that higher blowing ratios are correlated with lower temperatures further downstream of the SS4 (located at $s/s_{max} = 0.36$), indicating that increased cooling happens both locally and downstream at higher M values. The overall film effectiveness plots (Figure 16) support this conclusion. Local values at the highest blowing ratio were around $\phi = 0.7$, while local values at the lowest blowing ratio were around $\phi = 0.5$. Furthermore, this also holds true downstream of SS4, with ϕ values continuing to increase with an increase in M.

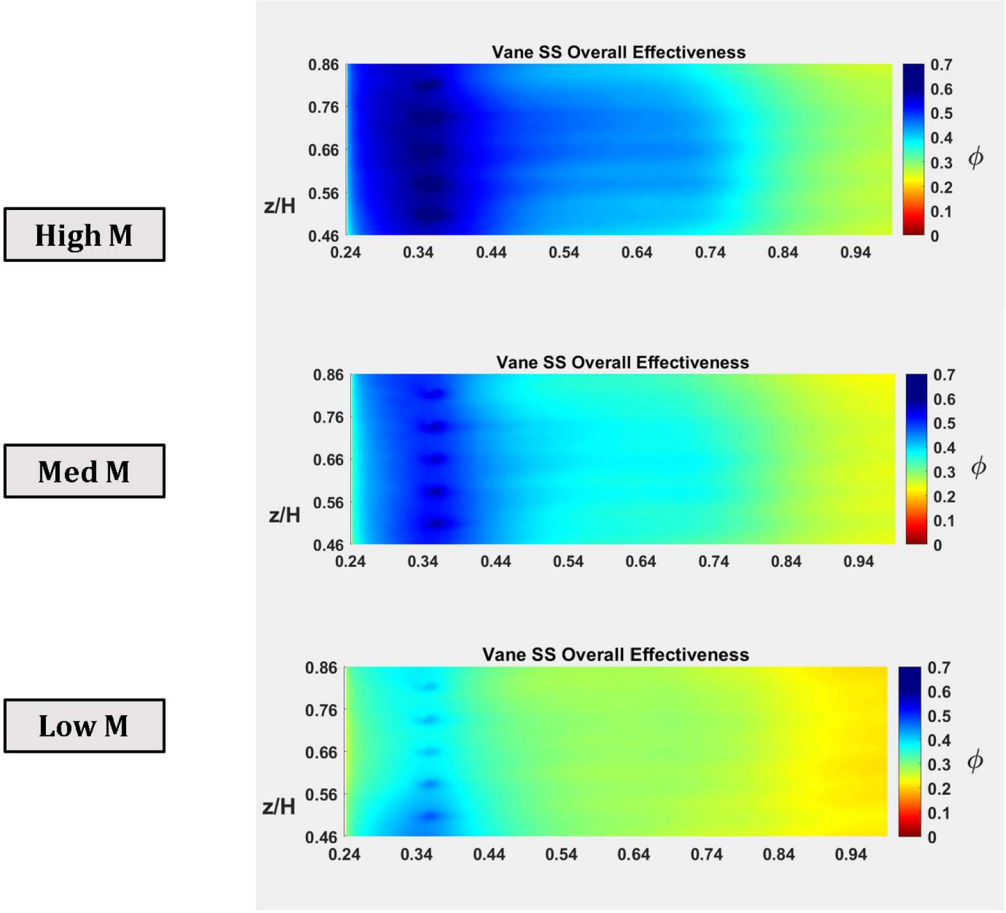

Figure 16. Vane SS Overall Film Effectiveness at High, Med, and Low M

The pressure side IR images captured the showerhead cooling and pressure side convective cooling holes. Raw IR images indicated the same trends shown by the suction side, which is increased surface cooling as values of M increase.

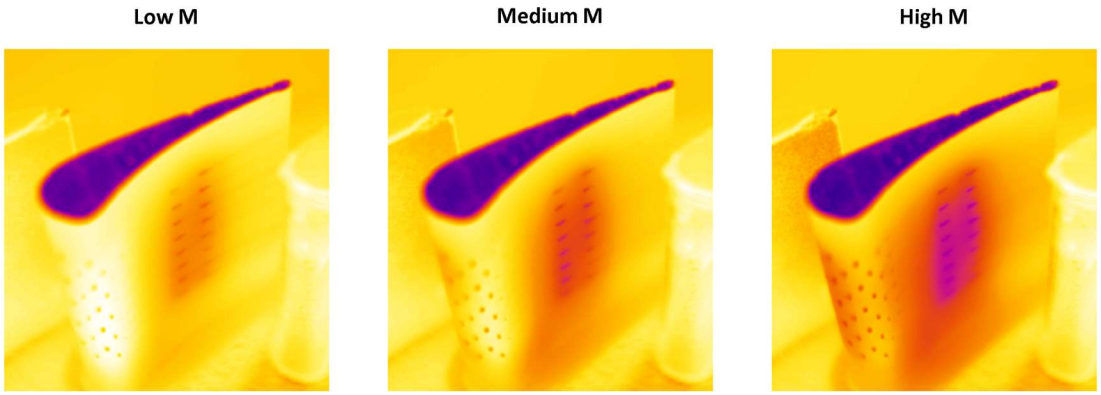

Figure 17. Raw IR Images of Vane Pressure Side

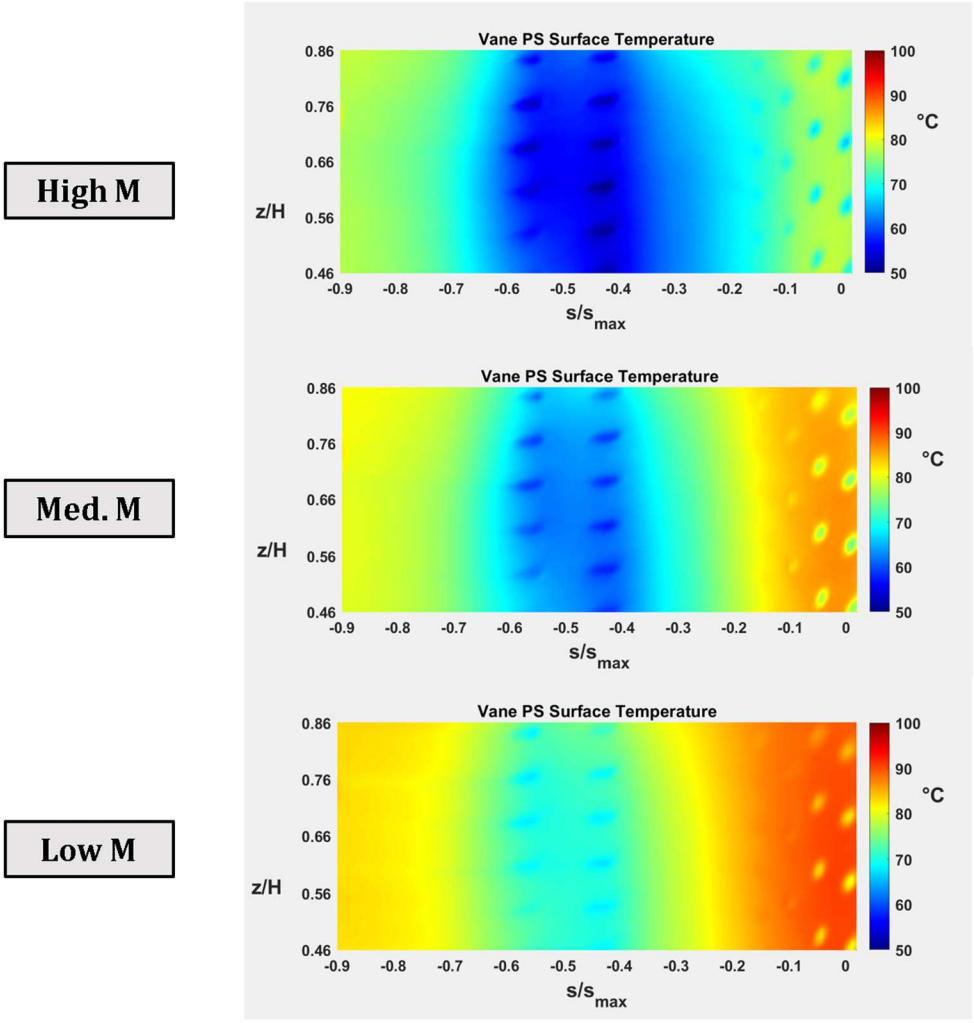

Figure 18. Vane PS Surface Temperature at High, Med, and Low M

Similar trends can be seen on the pressure side. Comparing the temperature contour plots (Figure 18), it is shown that higher blowing ratios are correlated with lower temperatures locally at hole locations and downstream of the holes, including in the area in between the showerhead cooling and convective holes. The overall film effectiveness plots (Figure 19) support this conclusion. Local values at the highest blowing ratio were around ϕ = 0.4 in the showerhead region and ϕ = 0.7 for PS4 and PS5, while local values at the lowest blowing ratio were around ϕ = 0.25 and ϕ = 0.5 for those regions respectively. Furthermore, the highest blowing ratio shows an significant increase in ϕ in the region between s/s_{max} = -0.1 and s/s_{max} = -0.4, indicating a reduction of "hot spots" in the area between the showerhead and convective cooling holes.

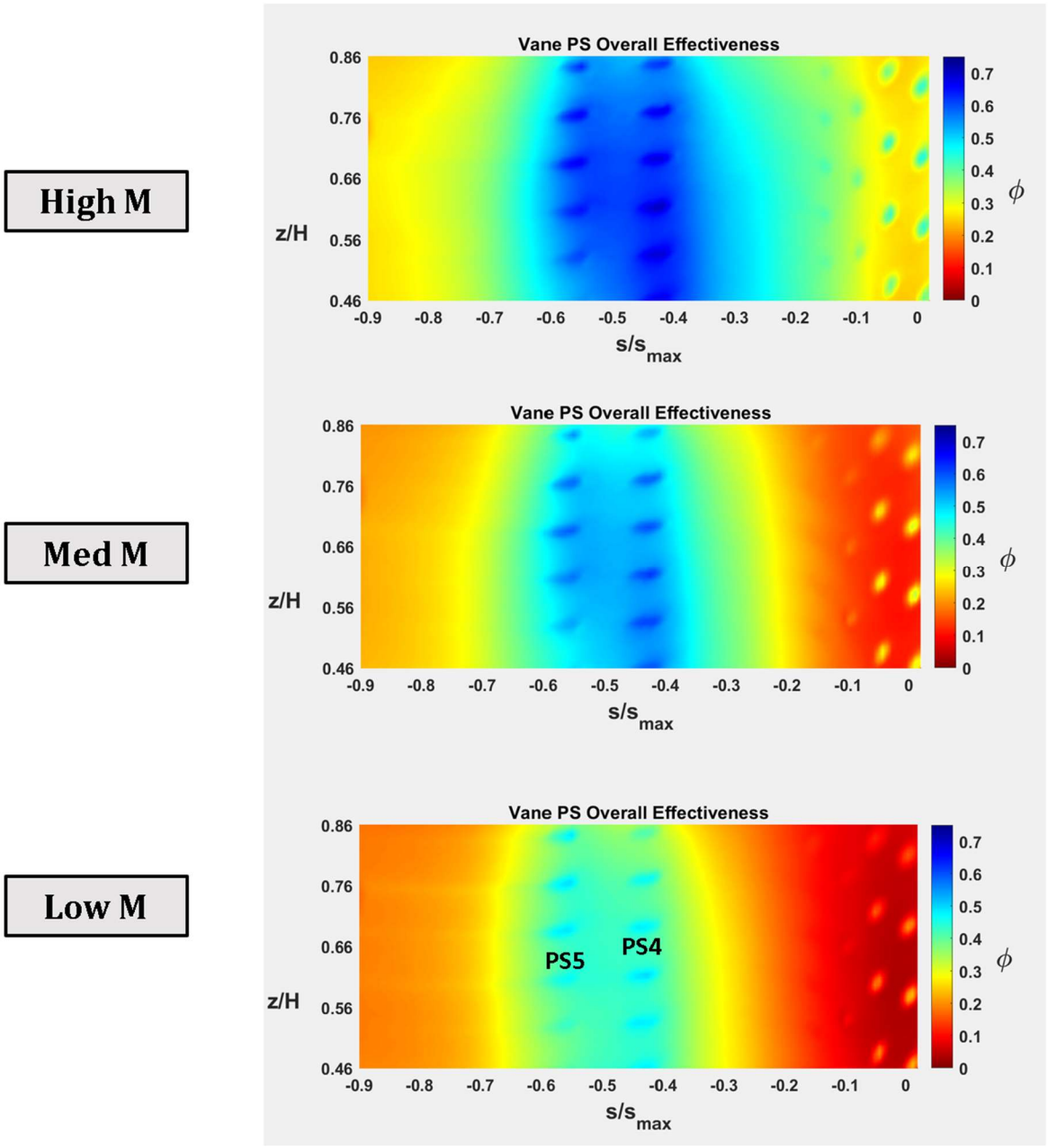

Figure 19. Vane PS Overall Film Effectiveness at High, Med, and Low M

Laterally averaged values of $\bar{\phi}$ over the spanwise direction (z/H) (corresponding to Figure 16 and Figure 19) are shown in Figure 20 to compare the average overall film effectiveness at different streamwise values on the suction side and pressure side. Comparing $\bar{\phi}$

at the different blowing ratios tested (both SS and PS), local increases in $\bar{\phi}$ are demonstrated at each hole location in Figure 20. The same graph is shown in Figure 21, but at positions of s/d for comparison. At the low and medium blowing ratios, PS2 and PS3 have little impact on $\bar{\phi}$, but at the highest blowing ratio, small spikes in the graph show a contribution to $\bar{\phi}$ from these hole locations.

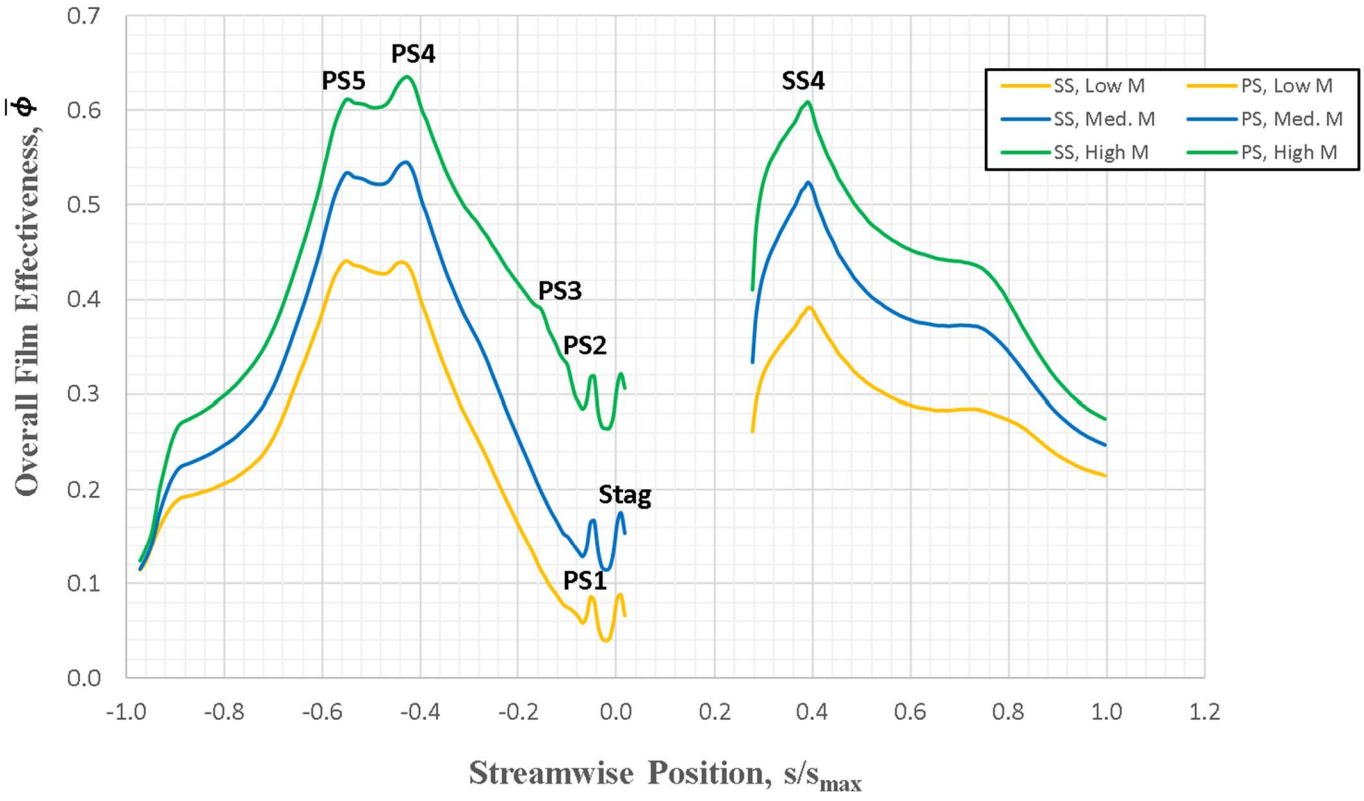

Figure 20. $\bar{\phi}$ vs (s/s$_{max}$) for all Measured Blowing Ratios

Values of $\bar{\phi}$ on the suction side are overall lower than values on the pressure side, which is as expected due to higher local velocities causing increased convection of the hot mainstream gas onto the part surface. This trend is similar to the results of Nathan, et al. [3] shown in Figure 22, where PS values of $\bar{\phi}$ are higher on average than SS values of $\bar{\phi}$. In Nathan, et al. [3],

momentum flux values were used as opposed to blowing ratios. The corresponding blowing ratios to the momentum flux values used were significantly higher than in this current study, as shown in Table 8. However, despite that, the trend of higher blowing ratios corresponding to higher overall film effectiveness values is consistent between the results of this paper and the results of Nathan, et al. [3]. Additionally, ϕ was observed to be more sensitive to blowing ratio increases than it was in Nathan, et al. [3].

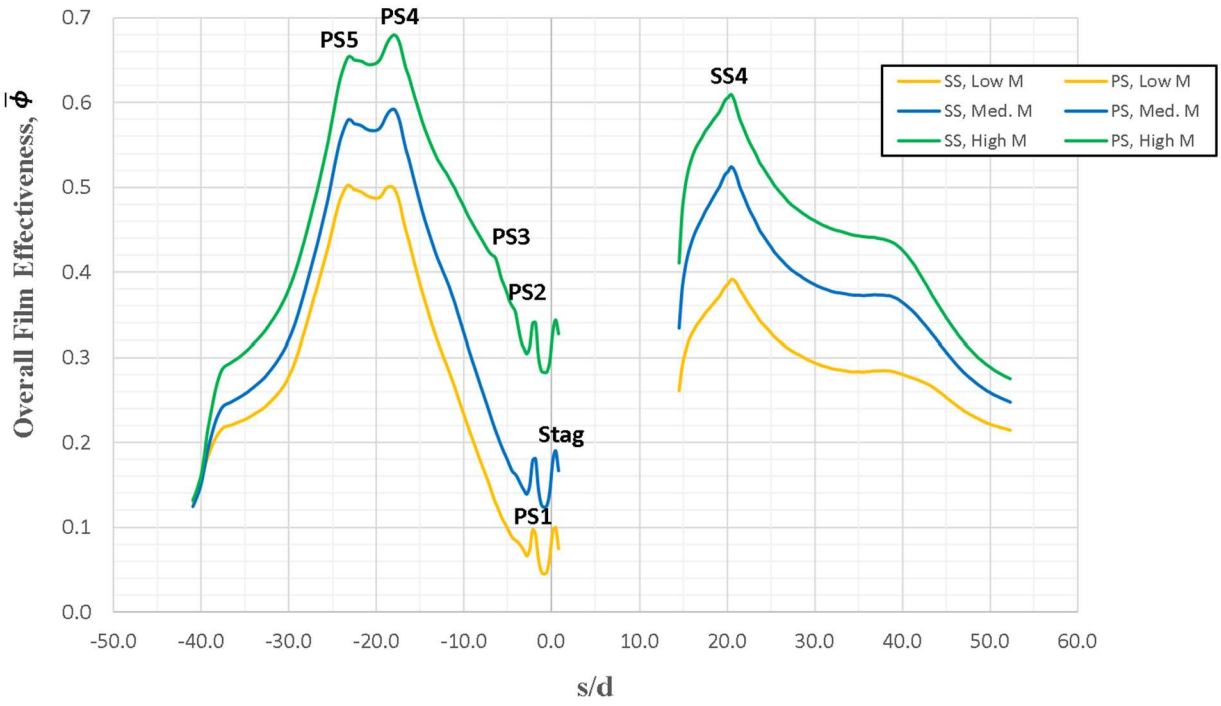

Figure 21. $\bar{\phi}$ vs (s/d) for all Measured Blowing Ratios

Table 8. Corresponding M* for I* from values used in Nathan, et al. [3]

I*	M_{SH}*	M* SS3	M* SS2	M* SS1	M* Stag	M* PS1	M* PS2	M* PS3
0.76	1.0	1.06	1.15	0.96	0.90	0.95	1.03	1.51
2.99	2.0	1.69	2.08	1.98	1.95	1.97	2.01	2.89
6.70	3.0	2.39	3.05	2.99	2.97	2.98	3.01	4.30

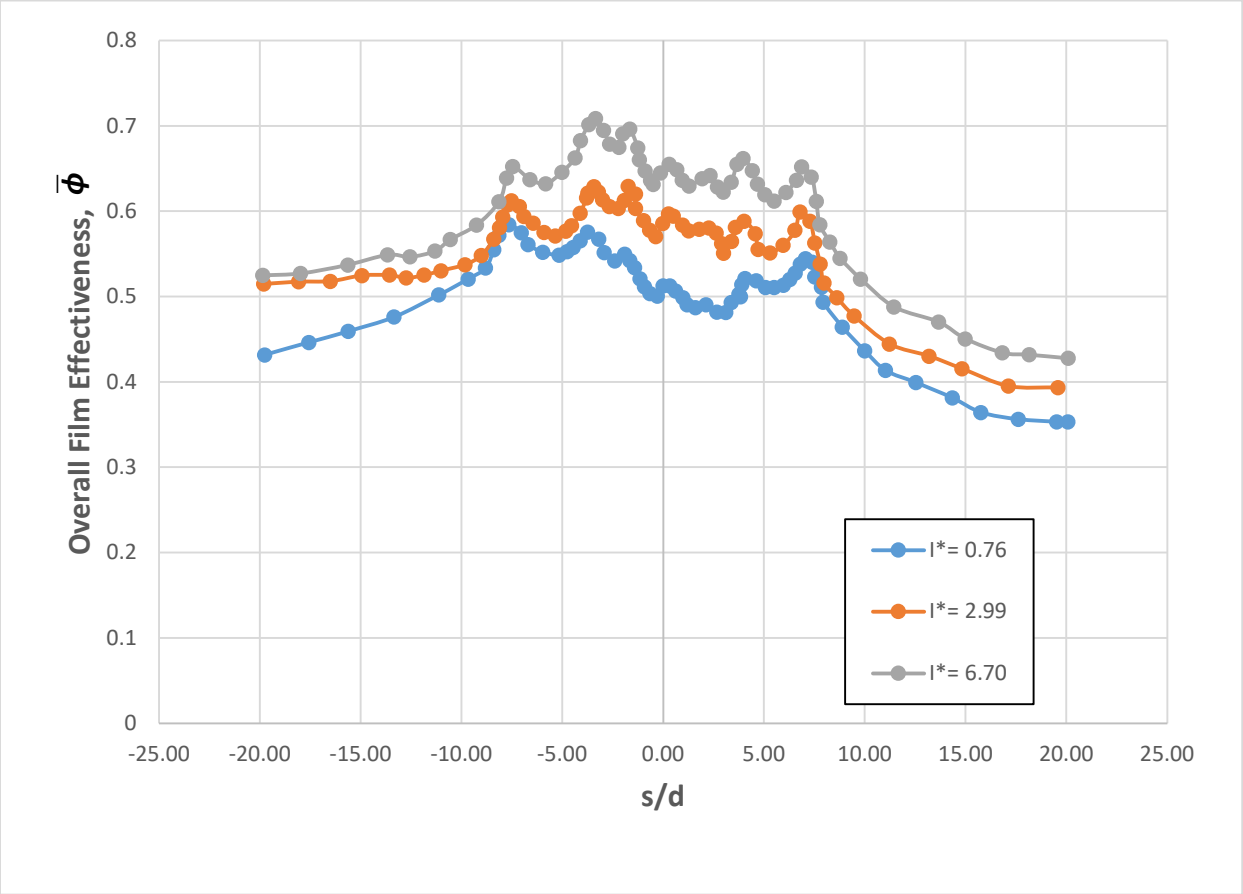

Figure 22. $\bar{\phi}$ vs (s/d) from the Results of Nathan, et al. [3]

Chapter 5: Conclusions

In this experimental study, measurements of overall film effectiveness in a scaled C3X turbine vane were made using low, medium, and high blowing ratios at transonic speeds. This study provides an experimental dataset of overall film cooling effectiveness at transonic speeds to better understand the performance and key differences of film cooling holes at these speeds. Additionally, overall film effectiveness measurements collected in this experiment are compared to expected results of similar geometry tested at subsonic speeds.

Similar to past studies, increased coverage between both showerhead and convective cooling holes as blowing ratios increase was observed in the experiment. Likewise, there was overall better performance (higher ϕ values) of showerhead region and in values downstream of the holes with an increase in blowing ratio.

Similarities in expected trends were observed, especially in comparing the suction side to the pressure side, despite differences in blowing ratio values. Values of ϕ on the suction side are overall lower than values on the pressure side, which is likely due to SS local velocities being higher than in previous studies of a similar nature. Additionally, ϕ was observed to be more sensitive to blowing ratio increases than it was in past studies. Furthermore, despite using lower blowing ratios than Nathan, et al. [3] and Williams, et al. [4], ϕ values were shown to demonstrate the same trends while being lower on average . Overall, trends were as expected in this experiment but used lower blowing ratios than in past literature, indicating a need for more data of overall film effectiveness at transonic speeds.

BIBLIOGRAPHY

[1] Dyson, Thomas E., Bogard, David G., and Bradshaw, Sean D. Evaluation of CFD simulations of film cooling performance on a turbine vane including conjugate heat transfer effects, International Journal of Heat and Fluid Flow, Volume 50, 2014, Pages 279-286, ISSN 0142-727X, https://doi.org/10.1016/j.ijheatfluidflow.2014.08.010.

[2] Hylton, L. D., Milhec, M. S., Turner, E. R., Nealy, D. A., and York, R. E., 1983, “Analytical and Experimental Evaluation of the Heat Transfer Distribution Over the Surface of Turbine Vanes,”, NASA, Contractor Report No. 168015.

[3] Nathan, M. L., Dyson, T. E., Bogard, D. G., and Bradshaw, Sean D. (September 26, 2013). "Adiabatic and Overall Effectiveness for the Showerhead Film Cooling of a Turbine Vane." ASME. J. Turbomach. March 2014; 136(3): 031005. https://doi.org/10.1115/1.4024680

[4] Williams, R. P., Dyson, T. E., Bogard, D. G., and Bradshaw, Sean D. (September 26, 2013). "Sensitivity of the Overall Effectiveness to Film Cooling and Internal Cooling on a Turbine Vane Suction Side." ASME. J. Turbomach. March 2014; 136(3): 031006. https://doi.org/10.1115/1.4024681

[5] Zuccarello, J, Saltzman, D, Lynch, S, Haydt, S, & Whitfield, C. "A Steady Transonic Linear Cascade for True Scale Cooling Measurements." Proceedings of the ASME Turbo Expo 2020: Turbomachinery Technical Conference and Exposition. Volume 7C: Heat Transfer. Virtual, Online. September 21–25, 2020. V07CT13A001. ASME. https://doi.org/10.1115/GT2020-14269

[6] Mick, W. J., and Mayle, R. E. (January 1, 1988). "Stagnation Film Cooling and Heat Transfer, Including Its Effect Within the Hole Pattern." ASME. J. Turbomach. January 1988; 110(1): 66–72. https://doi.org/10.1115/1.3262169

[7] Cutbirth, J. M., and Bogard, D. G. (April 9, 2002). "Thermal Field and Flow Visualization Within the Stagnation Region of a Film-Cooled Turbine Vane." ASME. J. Turbomach. April 2002; 124(2): 200–206. https://doi.org/10.1115/1.1451086

[8] Albert, JE, Bogard, DG, & Cunha, F. "Adiabatic and Overall Effectiveness for a Film Cooled Blade." Proceedings of the ASME Turbo Expo 2004: Power for Land, Sea, and Air. Volume 2: Turbo Expo 2004. Vienna, Austria. June 14–17, 2004. pp. 251-259. ASME. https://doi.org/10.1115/GT2004-53998

[9] Bacci, T.; Picchi, A.; Facchini, B. Flat Plate and Turbine Vane Film-Cooling Performance with Laid-Back Fan-Shaped Holes. Int. J. Turbomach. Propuls. Power 2019, 4, 14. https://doi.org/10.3390/ijtpp4020014

[10] Anderson, JB, Boyd, EJ, & Bogard, DG. "Experimental Investigation of Coolant-to-Mainstream Scaling Parameters with Cylindrical and Shaped Film Cooling Holes." Proceedings of the ASME Turbo Expo 2015: Turbine Technical Conference and Exposition. Volume 5B: Heat Transfer. Montreal, Quebec, Canada. June 15–19, 2015. V05BT12A033. ASME. https://doi.org/10.1115/GT2015-43072

[11] Ligrani, P. M., Saumweber , C., Schulz , A., and Wittig, S. (February 1, 2001). "Shock Wave–Film Cooling Interactions in Transonic Flows ." ASME. J. Turbomach. October 2001; 123(4): 788–797. https://doi.org/10.1115/1.1397305

[12] Gritsch, M., Schulz, A., and Wittig, S. (July 1, 1998). "Adiabatic Wall Effectiveness Measurements of Film-Cooling Holes With Expanded Exits." ASME. J. Turbomach. July 1998; 120(3): 549–556. https://doi.org/10.1115/1.2841752

ACADEMIC VITA

EDUCATION

Concurrent Degrees: B.S. Mechanical Engineering and B.S. Aerospace Engineering
Minors: Entrepreneurship and Innovation and IST for Aerospace Engineers
Schreyer Honors College | Leonhard Scholar
The Pennsylvania State University, University Park, PA **Graduation: May 2023**
Honors: Boeing Outstanding ME Junior Award, ASME International Gas Turbine Scholarship, Lockheed Martin STEM Scholarship, Phi Rho Merit Scholarship

Exchange Semester, Universidad de Navarra **Jan. – May 2022**
TECNUN School of Engineering, San Sebastian, Spain

LANGUAGES
Spanish - *Speaking*: Fluent, *Reading*: Fluent, *Writing*: Proficient

SOFTWARE
SolidWorks | Siemens NX | Creo | C++ | MATLAB | Python | SQL | Ansys | Labview

ENGINEERING EXPERIENCE

Propulsion Engineering Internship **June – Aug. 2022**
Hermeus Corporation, Atlanta, GA
- Defined requirements and created fluid schematic for hydrostatic testing stand
- Modeled hydrostatic testing stand component layout, tubing, and corresponding blast stand in Nx
- Sourced parts, created manufacturing plan, and built hydrostatic proof testing stand and blast stand
- Analyzed thermal strain and failure modes of exhaust nozzle transition section

Engineering Propulsion Lab Internship **May – Aug. 2021**
Lockheed Martin Space, Littleton, CO
- Created fluid schematic, testing procedure, and testing ops for flow capabilities for a propellant filter
- Designed skid with multiple design and mobility requirements for pressure chamber test stand
- Analyzed potential failure modes of ordnance test equipment

Propulsion Components Build Reliability Internship **Jan. – May 2021**
SpaceX, Hawthorne, CA
- Designed inspection tooling for a valve in Siemens NX, sourced parts, and manufactured tooling
- Owned and developed new flight-like testing conditions for a valve by reviewing flight data, automating test through scripting, and designing new test stand
- Performed a root cause analysis on a valve with gross leakage and subsequently tested piece parts to disposition cause and gather data on valve performance
- Created testing and python script to collect data and automatically analyze force testing on a valve

Process and Quality Engineering Internship **June – Aug. 2020**
Brentwood Industries, Reading, PA

- Assessed manufacturing non-conformance to determine if non-conforming part can still be used
- Performed Attribute Agreement Analysis using Minitab on several gages
- Updated quality inspection plans and transferred 80% of plans to a new system

RESEARCH EXPERIENCE

Experimental and Computational Convection Lab **Jan. 2020 – Present**
Pennsylvania State University, University Park, PA

- Conducting thesis research on turbine vane film cooling effectiveness in transonic flow conditions
- Modeled optimized film cooling holes in a C3X airfoil to collect data on film cooling effectiveness

Aircraft Propulsion Research Group **Aug. 2021 – Dec. 2021**
Pennsylvania State University, University Park, PA

- Created correlation based computational tool for optimized compressor blade design
- Wrote code for a computational tool to be used in estimating body force effects on flow around blade

LEADERSHIP & INVOLVEMENT

Officer of Member Relations, Society of Women Engineers (2019-23)
Lead and Mentor, Women in Engineering Program Orientation (2019-23)
Propulsion Team, PSU Human Powered Aircraft/Sailplane Team & Class (2020-23)
Honors Engineering Design Teaching Assistant, Penn State College of Engineering (2020)